Geophysical Research Letters

RESEARCH LETTER
10.1029/2019GL085359

Collisionless Magnetic Reconnection in an Asymmetric Oxygen Density Configuration

Håkon Midthun Kolstø[1], Michael Hesse[1,2], Cecilia Norgren[1], Paul Tenfjord[1], Susanne Flø Spinnangr[1], and Norah Kwagala[1]

[1]Space Plasma Physics Group, University of Bergen, Bergen, Norway, [2]Southwest Research Institute, San Antonio, TX, USA

Key Points:
- Alfvén scaling does not result in an adequate description of the reconnection rate due to the O^+ being demagnetized
- Scaling relation of reconnection rate for an asymmetrically distributed demagnetized species involves the average of the inflowing populations
- Significant asymmetry of the Hall electric field and the diffusion region

Correspondence to:
H. M. Kolstø,
hakon.kolsto@uib.no

Citation:
Kolstø H. M., Hesse M., Norgren C., Tenfjord P., Spinnangr S. F., & Kwagala N. (2020). Collisionless magnetic reconnection in an asymmetric oxygen density configuration. *Geophysical Research Letters*, *47*, e2019GL085359. https://doi.org/10.1029/2019GL085359

Received 13 SEP 2019
Accepted 2 DEC 2019
Accepted article online 3 JAN 2020

Abstract Combined with the magnetic field, the distribution of charged particles in the inflow region is expected to control the rate of magnetic reconnection. This paper investigates how the reconnection process is altered by a cold, asymmetrically distributed, oxygen population, which is initially located away from the current layer in the inflow regions. A particle-in-cell simulation is used to gain further insight into the dynamics of the system. The time evolution of the reconnection process proceeds rapidly compared to the cyclotron period of O^+. Therefore, the oxygen remains, to a good approximation, demagnetized. Thus, Alfvén scaling is not an adequate description of the reconnection rate. A scaling relation for the reconnection rate for an asymmetrically distributed, demagnetized species has been developed. Additionally, we find that an asymmetric density configuration leads to a distinct motion of the reconnection site and generates an asymmetry of the diffusion region and the Hall electric field.

1. Introduction

Magnetic reconnection is one of the most important energy release and transport processes in plasmas. In the Earth's magnetosphere, magnetic reconnection at the magnetopause is the primary mechanism responsible for the transport of energy, mass, momentum, and magnetic flux into Earth's magnetic cavity. Magnetic reconnection involves a violation of the ideal frozen-in condition (Vasyliunas, 1975), where the bulk motion of the particle species separates from the transport of magnetic flux.

In addition to the more abundant plasma species, that is, protons and electrons, heavier species, such as oxygen, may also be present in the plasma sheet as a result of ionospheric outflow (e.g., Baker et al., 1982; Chappell et al., 1987; Moore et al., 2001). The cold magnetotail oxygen originates from high-latitude ionosphere, and the ionospheric outflow rate is proportional to geomagnetic activity (Baker et al., 1982). Presence of oxygen of ionospheric origin in the Earth's magnetotail is supported by various observations (e.g., Frank et al., 1977; Grande et al., 2013; Moore et al., 2001; Mouikis et al., 2018; Wilken et al., 1995; Zong et al., 1998). Spacecraft observations reveal that oxygen may be the dominating ion species during storm time conditions (Kistler et al., 2005; Wygant et al., 2005a). At certain times, north-south asymmetries of ionospheric outflow may generate asymmetric oxygen inflow densities, and such asymmetries are also quite generically expected at the Earth's magnetopause (Li et al., 2013).

The inclusion of additional ion populations introduces distinctive kinetic behavior and different spatial and time scales for the system (Divin et al., 2016; Shay & Swisdak, 2004; Toledo-Redondo et al., 2015). The presence of heavy magnetized ions may result in a reduction of the Alfvén velocity, thus indicating a reduction of the reconnection rate (Hesse & Birn, 2004; Shay & Swisdak, 2004). Different mechanisms to slow down the reconnection rate have previously been proposed such as the effect of the tearing growth rate in the presence of O^+ (Karimabadi et al., 2011) and induced charge separation (i.e., *ambipolar* electric fields) (Liang et al., 2016, 2017). Previous studies (Tenfjord et al., 2018, 2019), investigated the effects of oxygen being symmetrically distributed in the inflow regions and proposed a scaling relation for the inclusion of a demagnetized species. Cluster reported density composition of $n_p = 0.03$ cm^{-3} and $n_{O^+} = 0.07$ cm^{-3} for protons and oxygen in the current sheet, respectively, (Wygant et al., 2005b) leading to a reduction of the reconnection rate of a factor of 6.3 through mass-loading effects and a factor of 3.3 for the proposed scaling relation (Tenfjord et al., 2019). During some phase of the evolution, this might imply that the dynamics of geomagnetic storms and substorms evolves twice as fast as expected when oxygen is present. This paper examines the effects on magnetotail reconnection imposed by an asymmetrically distributed oxygen population.

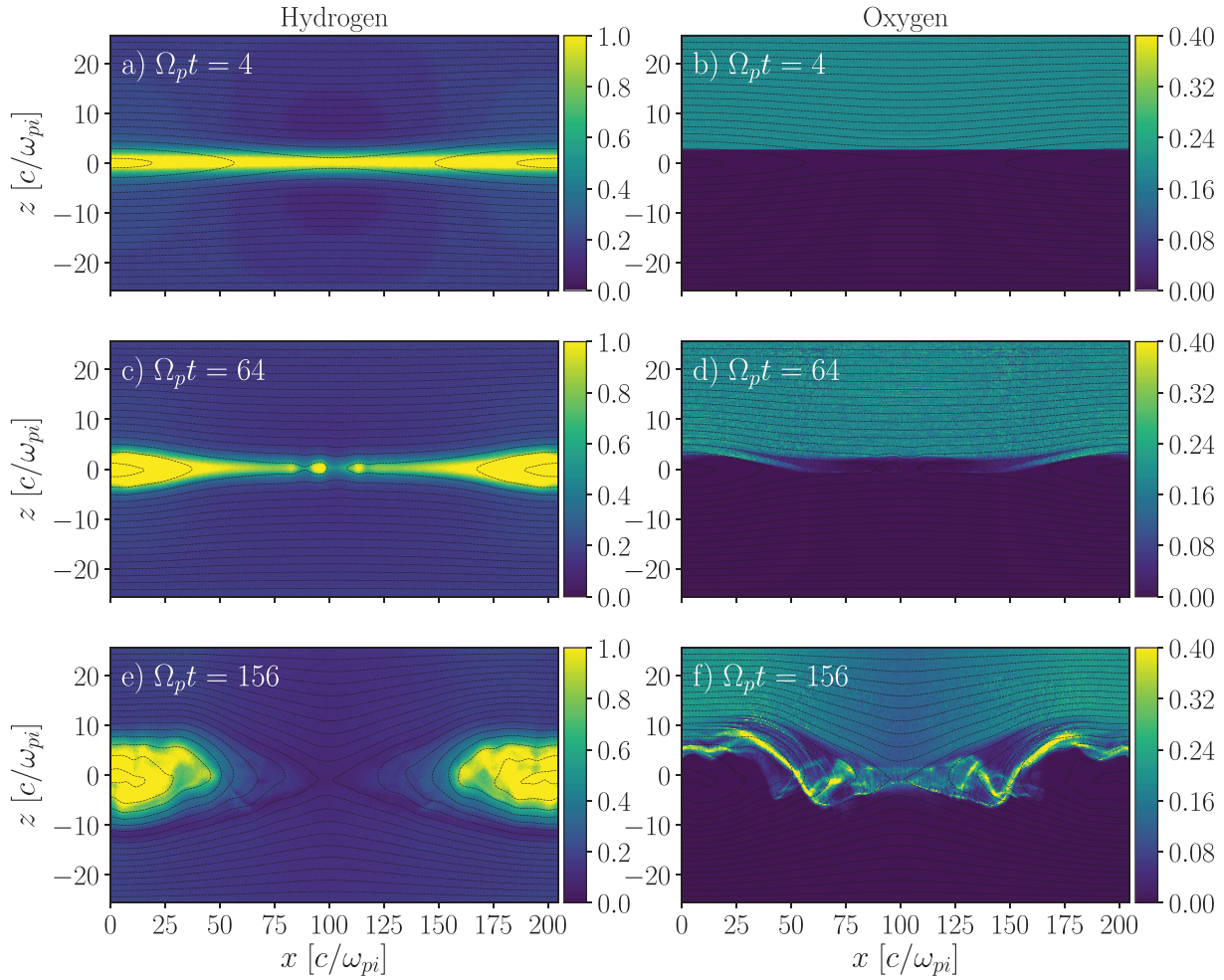

Figure 1. Time evolution for hydrogen (left: a, c, and e) and oxygen (right: b, d, and f) densities.

The outline of this paper is as follows: Section 2 will give an overview of the simulation setup employed for this study. Section 3 examines the evolution and dynamics of the reconnection site, for example, motion of x-point and the arising asymmetry of the diffusion region. Finally, in section 4 a scaling relation for an asymmetrically distributed, demagnetized, species is developed.

2. Simulation Setup

The analysis is performed by using a 2.5-D particle-in-cell (PIC) simulation, that is, two spatial components and three-fields and velocity components, designed to model the evolution of a current sheet subjected to asymmetric oxygen inflow. Initially, the configuration of the magnetic field is given as a two-dimensional generalized Harris-type equilibrium (see Hesse and Birn, 2004 for details) defined as $B_x = B_0 \tanh(z/\lambda)$, where $\lambda = 2d_p$ is the half width of the initial current sheet. The factor $d_p = c/\omega_{pi} (= c\sqrt{m_p/4\pi n_0 e^2})$ is the proton inertial length, where n_0 is the foreground density at the center of the initial current sheet.

In the upper inflow region (top lobe), oxygen O^+ is homogeneously distributed with a number density of $n_{O^+} = 0.2$ at a distance of $z > 2.5d_p$, where $z = 0$ is the initial location of the x-line (see Figure 1b). Density is normalized to n_0. Initially, the oxygen has zero thermal and bulk velocity. In addition to the oxygen, a uniform proton H^+ with a density of $n_b = 0.2$ is added to the Harris-sheet density configuration ($n_p = n_0/\cosh^2(z/2d_p) + n_b$) resulting in a peak density of 1.2 in the current layer.

The following mass ratios are employed: $m_p/m_e = 25$ for the protons/electrons and $m_{O^+}/m_p = 16$ for the oxygen/protons. A total of $4.8 \cdot 10^9$ macroparticles are used. Boundary conditions are periodic at $x = x_{\min}$

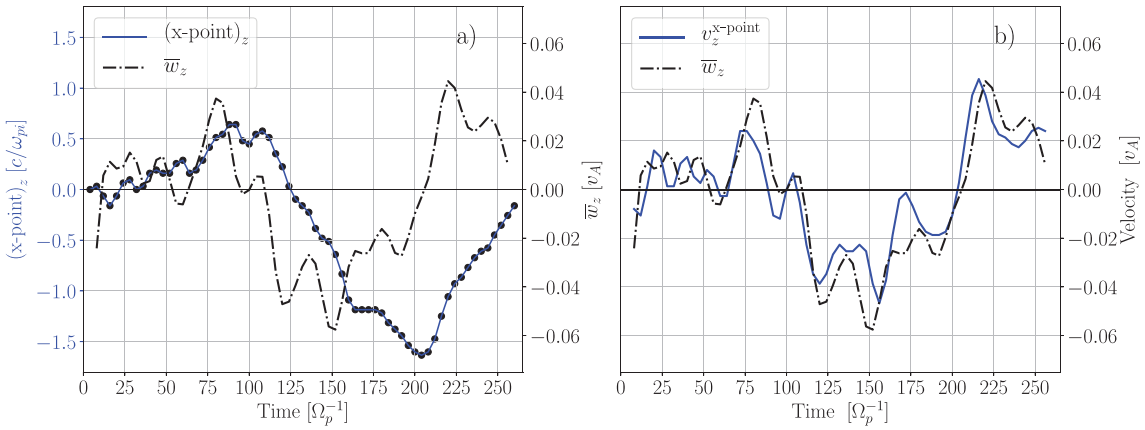

Figure 2. (a) Dynamics of the z-location of the x-point with respect to time shown by the blue dotted line and the average flux velocity shown by the black dash-dotted line. (b) Comparison of flux velocity (black dash-dotted) and velocity of the x-point (blue solid).

and $x = x_{\max}$. At $z = z_{\min}$ and $z = z_{\max}$, specular reflection is enabled and the out-of-plane electric field E_y is set to zero, preserving magnetic flux in the simulation domain.

Lengths are normalized to d_p, whereas time is normalized to the inverse of the proton cyclotron frequency $\Omega_p^{-1} = m_p/eB$. The size of our simulation domain is $200 \times 50\ d_p$ with a grid size of $3{,}200 \times 1{,}600$. We employ a time step of $\Omega_e \delta t = 0.5$. The velocity normalization is the proton Alfvén speed, based on the foreground current sheet density n_0. The foreground temperatures fulfill $T_p + T_e = 0.5$, in units of $[m_p v_A^2]$, derived from pressure balance

$$n_0(T_p + T_e) = \frac{B_0^2}{2}$$

with $n_0 = 1$ and $B_0 = 1$, and the ratio of proton-electron temperature is chosen to be $T_p/T_e = 5$. The ratio between the electron plasma frequency and gyrofrequency is $\omega_{pe}/\Omega_e = 2$.

3. Evolution and Dynamics of the Reconnection Site

In Figure 1, the O^+ and H^+ density are shown at three selected times. Close to the initial configuration, $\Omega_p t = 4$, oxygen is present in the inflow region only at a distance of $z > 2.5 d_p$. At $\Omega_p t = 64$ reconnection has initiated. However, the oxygen is still not present at the reconnection site. The reconnection rate peaks at $\Omega_p t = 80$, and an increasing amount oxygen is transported into the reconnection region, thus becoming present in the reconnection region. At $\Omega_p t = 156$ we observe horizontal layers of increased oxygen density close to the x-point. These striations form as a result of quasi-steady flow of oxygen from the inflow to the reconnection region (Tenfjord et al., 2018). Inclined oxygen density striations, which are evident at $\Omega_p t = 156$, are governed by the formation and expansion of the localized Hall electric field E_z. As the Hall electric field expands, oxygen particles at rest are collectively accelerated resulting in an oxygen density wave (Tenfjord et al., 2018).

3.1. Motion of the X-Point

The asymmetric oxygen distribution leads to distinct motion of the x-point across the initial x-line. The blue dotted line in Figure 2 shows the displacement of the x-point in the z direction with respect to time. We observe a shift of the x-point toward positive z, reaching a value of $z = 0.7 d_p$. From $\Omega_p t > 120$ the x-point moves in the negative z direction, reaching its minimum at $z = -1.7 d_p$. Close to the end of the simulation, the x-point moves toward its initial value. The two processes governing the shift toward positive and negative z values are distinct. We now examine them further.

We start by investigating how the shift of the x-point relates to the differences in the flux velocity between the top and bottom lobe. The motion of the magnetic flux in z direction is determined by finding the frame in which $\frac{dA_y}{dt} = 0$. This leads to the magnetic flux velocity w_z

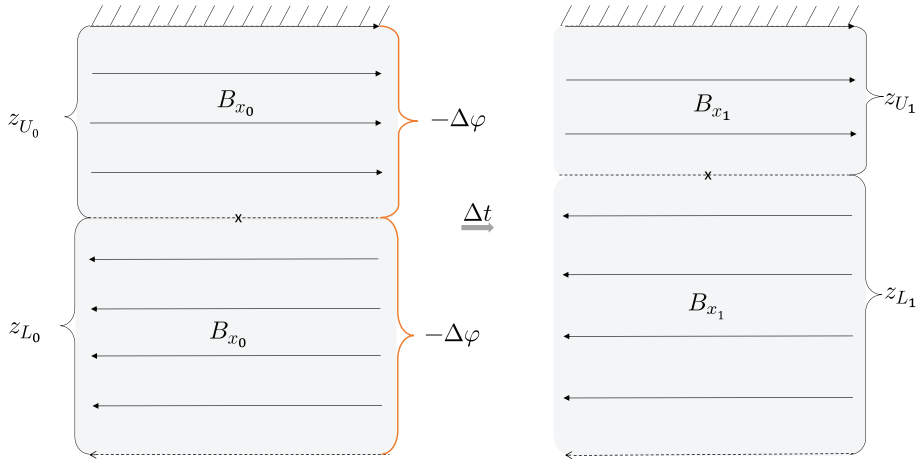

Figure 3. Reconnection site before (after) reconnection has initiated on left (right). The oxygen front is illustrated by the wall, hindering the replenishment of magnetic field lines.

$$\frac{\mathrm{d}A_y}{\mathrm{d}t} = \frac{\partial A_y}{\partial t} + w_z \frac{\partial A_y}{\partial z} = 0$$

which gives

$$w_z = -\left(\frac{\partial A_y}{\partial t}\right) / \left(\frac{\partial A_y}{\partial z}\right)$$

In order to investigate the correlation between the magnetic flux velocity and the actual velocity of the x-point, we average w_z throughout the simulation domain, excluding the diffusion region.

The velocity of the x-point should match any differences of the flux velocities in these two regions. The average flux velocity $\overline{w}_z$, shown in Figure 2, would be zero if the flux were transported in a convergent manner in the top and bottom lobes. The velocity of the x-point, $v_z^{\text{x-point}} (= \Delta z^{\text{x-point}}/\Delta t)$ (blue line) displays a rather good agreement with the average flux velocity $\overline{w}_z$, indicating that $v_z^{\text{x-point}}$ is dictated by the differences of w_z in the two inflow regions.

The difference in the magnetic flux velocities between the two inflow regions is attributed to a drag imposed by the higher inertia of the oxygen species. As the far more agile electrons move with the magnetic field, an (ambipolar) electric field is set up to prevent charge separation (Karimabadi et al., 2011; Liang et al., 2016). The resulting electric field impedes the transport of magnetic flux from the top lobe. However, in the lower inflow region, the absence of oxygen lets the electrons and protons move, to a higher extent, unencumbered toward the x-line.

The limited flux mobility in the region covered by cold oxygen results in an upward movement of the current layer. This can be shown analytically by approximating the oxygen region as nearly stationary such that the flux velocity and the overall plasma bulk velocity is much smaller here than elsewhere. The different regions of flux mobility above and below are indicated by z_U and z_L, see Figure 3. If magnetic reconnection removes the same amount of flux $\Delta\varphi$ from the upper region and the lower region, force balance requires that the current layer moves upward to keep the magnetic pressure equal on both sides. At a time t_1, indicated by the subscript, the flux contained in the two regions can be written as

$$B_{x_1} z_{U_1} = B_{x_0} z_{U_0} - \Delta\varphi \tag{1}$$

$$B_{x_1} z_{L_1} = B_{x_0} z_{L_0} - \Delta\varphi \tag{2}$$

where the numbered subscripts refer to the times of evaluation, t_0 and t_1. The length of the combined regions are to be remained constant, thus

$$z_{U_1} + z_{L_1} = z_{U_0} + z_{L_0} \tag{3}$$

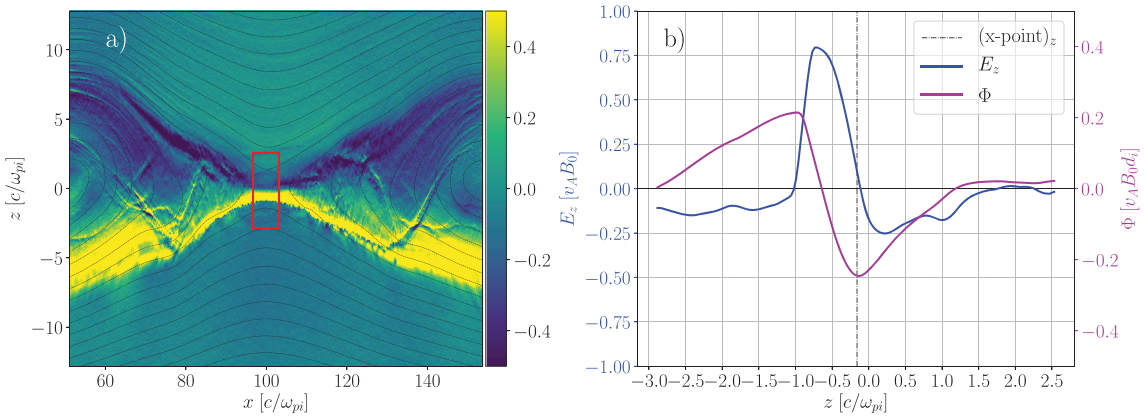

Figure 4. Asymmetry in the Hall electric field E_z at $\Omega_p t = 132$. E_z and Φ are evaluated inside the red box shown panel (a). The dashed line shows the z-location of the x-point for this time step.

Combining equations (1)–(3), the change in length of the upper and lower regions can now be expressed as

$$z_{U_1} - z_{U_0} = \frac{\Delta\varphi}{B_{x_1}} \left[\frac{2z_{U_0}}{z_{U_0} + z_{L_0}} - 1 \right] < 0, \quad \text{as} \quad 2z_{U_0} < z_{U_0} + z_{L_0} \tag{4}$$

$$z_{L_1} - z_{L_0} = \frac{\Delta\varphi}{B_{x_1}} \left[\frac{2z_{L_0}}{z_{U_0} + z_{L_0}} - 1 \right] > 0, \quad \text{as} \quad 2z_{L_0} > z_{U_0} + z_{L_0} \tag{5}$$

Equations (4) and (5) imply that the x-point shifts to positive values of z. In order to reach equilibrium, the upper region needs to be compressed and the lower region expanded, leading to an upward motion of the current layer (see Figure 3).

The x-point reaches its highest value at $\Omega_p t = 88$ and is thereafter shifted toward negative z due to a different process. The Hall electric field E_z extends into the upper lobe and accelerates the demagnetized oxygen toward the x-point, resulting in an increase of the dynamic oxygen pressure. At this point the oxygen no longer imposes a drag on the transport of magnetic flux, but instead contributes to an increase of w_z as a result of its enhanced dynamic pressure, see Figure 5. An overall higher w_z on the oxygen side, compared to the southern lobe, shifts the x-point to negative z-values. In the next section we will see how the increase of the dynamic pressure affects the diffusion region.

3.2. Asymmetry of the Diffusion Region

As the oxygen gets involved in the reconnection process, an asymmetry in the diffusion region arises. Figure 4 shows an overview of the Hall electric field and its potential. Figure 4a shows the structure of the Hall E_z, and in Figure 4b a clear asymmetry across the diffusion region is evident.

To investigate the asymmetry of the Hall electric field E_z we start by examining the pressure balance along z through the x-point. We obtain

$$P^o_{zz} + P^p_{zz} + P^e_{zz} + m_{O^+} n^{\text{avg}}_{O^+} v^2_{O^+ z} + \frac{B_x^2}{2\mu_0} \sim C \tag{6}$$

Equation (6) only includes the dominant contributions (shown for $\Omega_p t = 132$ in Figure 5) where C is a constant, and $n^{\text{avg}}_{O^+}$ is the average oxygen density. In Figure 5, we see that the contribution to the overall pressure balance of the dynamic and thermal pressures for both oxygen and protons are substantially higher in the northern lobe than in the southern lobe. On the $z > 0$ side a clear reduction of the gradient of the magnetic pressure is seen. Additionally, asymmetries in the dynamic oxygen pressure and the thermal pressure of both the oxygen and protons are found.

Due to acceleration of oxygen by the Hall electric field, the dynamic oxygen pressure increases and a reduction of the magnetic pressure arises to preserve the pressure balance. The higher contribution of the pressure terms from the plasma species in the northern lobe suppresses the contribution of the magnetic pressure

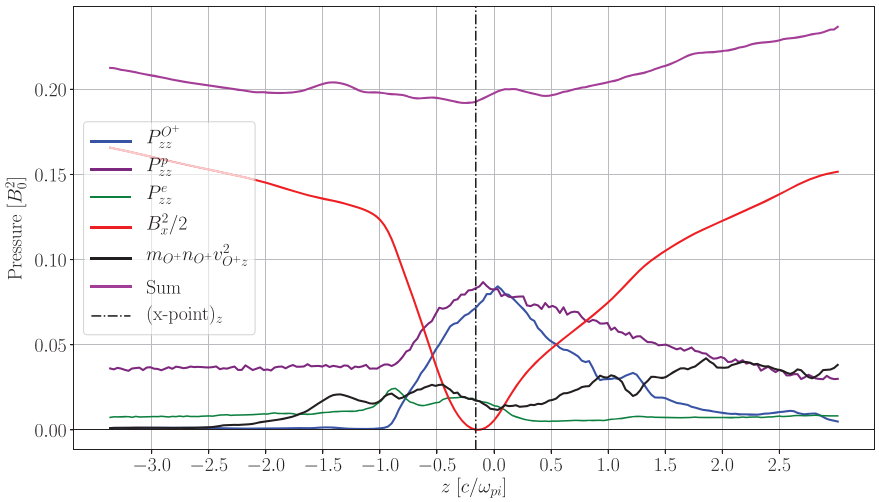

Figure 5. Pressure balance through x-point along z taken at time $\Omega_p t = 132$.

to preserve the pressure balance. The immediate effect of this is the broadening of the B_x profile which, through Ampères law $\mu_0 j_y \sim \partial/\partial_z B_x$, leads to a reduced current density. The reduction in the magnetic field strength results in a decrease of E_z in the northern lobes through Ohm's law.

In the region shown in Figure 5, the current is, to a good approximation, mainly carried by the far more agile electrons. We may therefore write the Hall electric field in the following manner

$$E_z \sim v_{ey} B_x \sim \frac{j_y}{n_e} B_x \sim \frac{1}{\mu_0 n_e} \left(\frac{\partial B_x}{\partial z} \right) B_x$$

which may be written, in terms of the magnetic pressure, in the following way

$$E_z \sim \frac{1}{n_e} \frac{\partial}{\partial z} \left(\frac{B_x^2}{2\mu_0} \right) \tag{7}$$

From equation (7) we see that the Hall electric field is directly dependent on the gradient of the magnetic pressure. Thus, on the oxygen side, the flatter profile of the magnetic pressure results in a smaller gradient and thereby reducing the Hall electric field.

4. Scaling of the reconnection rate

In this section we evaluate how the reconnection rate scales for asymmetrically distributed oxygen. There are several reasons to expect that the aforementioned configuration would affect the reconnection rate. Being under the influence of oxygen, we have seen that the flux velocity is reduced in the top lobe compared to the bottom lobe. Furthermore, the cyclotron period of the oxygen species is much longer than the characteristic time scale of the reconnection process (Ω_p^{-1}), oxygen is therefore mainly influenced by electric forces. This can also be seen in Tenfjord et al. (2018), where a similar simulation setup is employed.

Mass loading effects predict a reduction in the reconnection rate that scales as the total Alfvén velocity, that is, $\sqrt{(m_{O^+} n_{O^+}/m_p n_p + 1)}$. However, Tenfjord et al. (2019) investigated how the reconnection rate scales in the presence of demagnetized oxygen and found that the reconnection rate was reduced much less. Performing a scaling analysis similar to that of Tenfjord et al. (2019) leads to a relation for the reconnection rate in the presence of an asymmetrically distributed oxygen density. The Hall electric field for the protons scales in the following manner

$$E_z \sim \frac{1}{q n_p} \frac{\partial}{\partial z} P_{zz}^p \sim \frac{1}{q n_p} \frac{P_{zz}^p}{L_{\text{Hall}}} \sim \frac{E_y}{\beta}$$

The factor β is a proportionality constant relating the off-diagonal pressure components to the diagonal components. We have here assumed that off-diagonal pressure components shows a linear dependence on

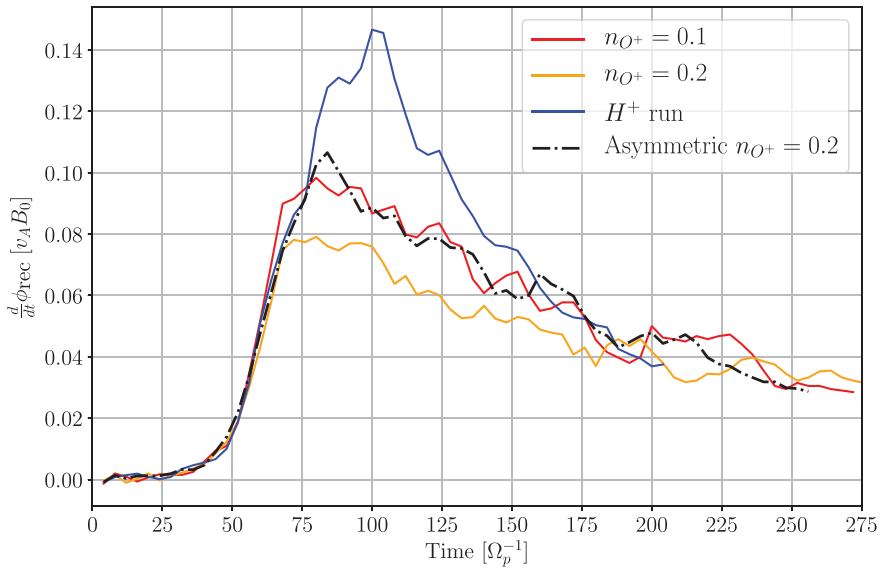

Figure 6. Comparison of the reconnection rates for runs with different oxygen densities. Clear agreement between the asymmetric oxygen density configuration (dash-dotted) $n_{\rm O^+} = 0.2$ run and the symmetric oxygen density configuration (red) $n_{\rm O^+} = 0.1$ run.

the trace of pressure tensor (Tenfjord et al., 2019). Similarly for the electrons

$$P^e_{zz} \sim q n_e L_{\rm EDR} \frac{E_y}{\alpha}$$

The acceleration of O^+ from one side leads to a bulk motion of oxygen inside the diffusion region. This expression differs from what used in Tenfjord et al. (2019), where O^+ existed in both lobes leading to two counterstreaming populations which manifested as pressure. For the oxygen species, the Hall electric field scales as

$$E_z \sim \frac{1}{q n^{\rm avg}_{\rm O^+}} \frac{\partial}{\partial z}(P^o_{zz} + m_{\rm O^+} n^{\rm avg}_{\rm O^+} v^2_{\rm O^+ z}) \sim \frac{1}{q n_{\rm O^+}} \frac{P^o_{zz} + m_{\rm O^+} n^{avg}_{\rm O^+} v^2_{\rm O^+ z}}{L_{Hall}}$$

Substituting the derived pressure relations into equation (6) gives

$$\frac{B_x^2}{2\mu_0} + q n_p L_{\rm Hall} \frac{E_y}{\beta} + q(n_p + n^{\rm avg}_{\rm O^+}) L_{\rm EDR} \frac{E_y}{\alpha} + q n^{\rm avg}_{\rm O^+} L_{\rm Hall} \frac{E_y}{\beta} \sim C$$

Writing out the average oxygen density to relate the density of the upper $n^U_{\rm O^+}$ and lower $n^L_{\rm O^+}$ lobes as $n^{\rm avg}_{\rm O^+} = \frac{1}{2}(n^U_{\rm O^+} + n^L_{\rm O^+})$ we get

$$E_y \left[e \left(\frac{L_{\rm Hall}}{\beta} - \frac{L_{\rm EDR}}{\alpha} \right) \left(n_p + \frac{n^U_{\rm O^+} + n^L_{\rm O^+}}{2} \right) \right] \sim C - \frac{B_x^2}{2\mu_0}$$

Neither the right-hand side, the scale lengths, nor the proportionality constants, α and β, depends on the oxygen density. This leads us to express the scaling relation of the reconnection electric field as a function of the oxygen and proton density

$$E_y \sim (1 + \frac{n^U_{\rm O^+} + n^L_{\rm O^+}}{2 n_p})^{-1} \tag{8}$$

In Figure 6, we compare the reconnection rate, which can be expressed as $\frac{\rm d}{{\rm d}t}\phi_{\rm rec} = \int E_y {\rm d}y$, to numerical simulations, hereafter referred to as runs, of different oxygen densities. The oxygen species are initially a distance of $2.5 d_p$ from the x-line for the three oxygen runs. The reconnection rate of the symmetric density configuration of $n_{\rm O^+} = 0.1$ (red) (Tenfjord et al., 2019) displays a good agreement with the asymmetric

density configuration of $n_{O^+} = 0.2$ (dash-dotted line). The blue solid line represents a run with absence of oxygen.

The scaling relation in equation (8) coincides with the reconnection rates as seen in Figure 6. All runs follow the same evolution toward the peak of the reconnection rate. This indicates that an increase of the density reduces the maximum value of the reconnection rate and not the rate at which it reaches its peak. This implies that the reconnection rate is determined by the oxygen content and not its initial configuration.

5. Discussion and Summary

Our results provide insight into the rate reconnection actually proceeds with. It further provides a generalization of the estimated reconnection rate when the plasma system includes heavier species in addition to the protons and electrons. This generalization is valid when heavier ion species are distributed asymmetrically, and such scenarios may occur for ionospheric outflow, for example, when the Northern Hemisphere is illuminated, and the Southern Hemisphere is in darkness. The smaller gyrofrequency of the O^+ introduces longer coupling time scales. Therefore, the oxygen is largely demagnetized on the time scales of this investigation and Alfvén scaling of the reconnection rate does not apply in our model. It should be noted that steady state reconnection lasting for a significantly longer time would be expected to magnetize the oxygen at some point, and Alfvén scaling may apply for these cases. Through pressure balance arguments, we succeeded in extending previous results (Tenfjord et al., 2018) to derive a scaling relation for the reconnection rate for an asymmetrically distributed, demagnetized, species.

The reconnection rate during the fast phase shows no dependency on the oxygen density. We have seen that reduction of the reconnection rate is dependent on the overall content of the demagnetized species and not its initial configuration. The initial temperature of oxygen is chosen to be zero to isolate oxygen inertia on the reconnection process from other effects, such as streaming and finite temperature. In Tenfjord et al. (2019) it was shown that an initial temperature of the O^+ has no significant effect on the reconnection rate. The additional effects arising from an asymmetric oxygen population, such as asymmetric E_z, bulk z-directed oxygen velocity in the diffusion region and motion of x-point, does not appear to have any significant effect on the reconnection rate.

Regarding observations, signatures as the oxygen striations seen in Figure 1 and asymmetries in the Hall fields should be detectable. The results obtained in this study may apply to magnetotail reconnection in case of north-south asymmetries of ionospheric outflow. In addition, they may play a role in reconnection at the magnetopause, even though many effects may be masked by the typical and often rather large asymmetries across the current layer. They may further apply to laboratory devices and other reconnection geometries, where either history or asymmetric particle injection may lead to similarly asymmetric situations. Regarding space applications, we hope our results provide useful insight for future analysis of space mission data, in particular, the Magnetospheric Multiscale mission.

Acknowledgments
This study was supported by the Research Council of Norway/ CoE University of Bergen, by NOTUR/NORSTOR under project NN9496K, and by NASA's MMS mission. Data set used in this analysis is available at (Kolstø, 2019).

References

Baker, D. N., Hones, E. W., Young, D. T., & Birn, J. (1982). The possible role of ionospheric oxygen in the initiation and development of plasma sheet instabilities. *Geophysical Research Letters*, *9*(12), 1337–1340. https://doi.org/10.1029/GL009i012p01337

Chappell, C. R., Moore, T. E., & Waite, J. H. (1987). The ionosphere as a fully adequate source of plasma for the Earth's magnetosphere. *Journal of Geophysical Research*, *92*(A6), 5896–5910. https://doi.org/10.1029/JA092iA06p05896

Divin, A., Khotyaintsev, Y. V., Vaivads, A., André, M., Toledo-Redondo, S., Markidis, S., & Lapenta, G. (2016). Three-scale structure of diffusion region in the presence of cold ions. *Journal of Geophysical Research: Space Physics*, *121*, 12,001–12,013. https://doi.org/10.1002/2016JA023606

Frank, L. A., Ackerson, K. L., & Yeager, D. M. (1977). Observations of atomic oxygen (O^+) in the Earth's magnetotail. *Journal of Geophysical Research*, *82*, 129–134. https://doi.org/10.1029/JA082i001p00129

Grande, M., Perry, C. H., Hall, A., Fennell, J., Nakamura, R., & Kamide, Y. (2013). What is the Effect of Substorms on the Ring Current Ion Population During a Geomagnetic Storm? *American Geophysical Union (AGU)*, 75–89. https://doi.org/10.1029/142GM08

Hesse, M., & Birn, J. (2004). On the cessation of magnetic reconnection. *Annales de Geophysique*, *22*(2), 603–612. https://doi.org/10.5194/angeo-22-603-2004

Karimabadi, H., Roytershteyn, V., Mouikis, C. G., Kistler, L. M., & Daughton, W. (2011). Flushing effect in reconnection: Effects of minority species of oxygen ions. *Planetary and Space Science*, *59*(7), 526–536. https://doi.org/10.1016/j.pss.2010.07.014

Kistler, L. M., Mouikis, C., Möbius, E., Klecker, B., Sauvaud, J. A., Réme, H., et al. (2005). Contribution of nonadiabatic ions to the cross-tail current in an O^+ dominated thin current sheet. *Journal of Geophysical Research*, *110*, A06213. https://doi.org/10.1029/2004JA010653

Kolstø H. M. (2019). Replication data for: Collisionless Magnetic Reconnection in an Asymmetric Oxygen Density Configuration, https://doi.org/10.18710/4YHU4R

Li, K., Haaland, S., Eriksson, A., André, M., Engwall, E., Wei, Y., et al. (2013). Transport of cold ions from the polar ionosphere to the plasma sheet. *Journal of Geophysical Research: Space Physics*, *118*, 5467–5477. https://doi.org/10.1002/jgra.50518

Liang, H., Ashour-Abdalla, M., Lapenta, G., & Walker, R. J. (2016). Oxygen impacts on dipolarization fronts and reconnection rate. *Journal of Geophysical Research: Space Physics*, *121*, 1148–1166. https://doi.org/10.1002/2015JA021747

Liang, H., Lapenta, G., Walker, R. J., Schriver, D., El-Alaoui, M., & Berchem, J. (2017). Oxygen acceleration in magnetotail reconnection. *Journal of Geophysical Research: Space Physics*, *122*, 618–639. https://doi.org/10.1002/2016JA023060

Moore, T. E., Chandler, M. O., Fok, M.-C., Giles, B. L., Delcourt, D. C., Horwitz, J. L., & Pollock, C. J. (2001). Ring Currents and Internal Plasma Sources. *Space Science Reviews*, *95*(1/2), 555–568. https://doi.org/10.1023/A:1005264907107

Mouikis, C. G., Kistler, L. M., Liu, Y. H., Klecker, B., Korth, A., & Dandouras, I. (2018). H^+ and O^+ content of the plasma sheet at 15–19 Re as a function of geomagnetic and solar activity. *Journal of Geophysical Research: Space Physics*, *115*, A00J16. https://doi.org/10.1029/2010JA015978

Shay, M. A., & Swisdak, M. (2004). Three-Species Collisionless Reconnection: Effect of O^+ on Magnetotail Reconnection. *Physical Review Letters*, *93*, 175001. https://doi.org/10.1103/PhysRevLett.93.175001

Tenfjord, P., Hesse, M., & Norgren, C. (2018). The Formation of an Oxygen Wave by Magnetic Reconnection. *Journal of Geophysical Research: Space Physics*, *123*, 9370–9380. https://doi.org/10.1029/2018JA026026

Tenfjord, P., Hesse, M., Norgren, C., Spinnangr, S. F., & Kolstø, H. (2019). The impact of oxygen on the reconnection rate. *Geophysical Research Letters*, *46*, 6195–6203. https://doi.org/10.1029/2019GL082175

Toledo-Redondo, S., Vaivads, A., André, M., & Khotyaintsev, Y. V. (2015). Modification of the Hall physics in magnetic reconnection due to cold ions at the Earth's magnetopause. *Geophysical Research Letters*, *42*, 6146–6154. https://doi.org/10.1002/2015GL065129

Vasyliunas, V. M. (1975). Theoretical models of magnetic field line merging. *Reviews of Geophysics*, *13*(1), 303–336. https://doi.org/10.1029/RG013i001p00303

Wilken, B., Zong, Q. G., Daglis, I. A., Doke, T., Livi, S., Maezawa, K., et al. (1995). Tailward flowing energetic oxygen ion bursts associated with multiple flux ropes in the distant magnetotail: GEOTAil observations. *Geophysical Research Letters*, *22*(23), 3267–3270. https://doi.org/10.1029/95GL02980

Wygant, J. R., Cattell, C. A., Lysak, R., Song, Y., Dombeck, J., McFadden, J., et al. (2005a). Cluster observations of an intense normal component of the electric field at a thin reconnecting current sheet in the tail and its role in the shock-like acceleration of the ion fluid into the separatrix region. *Journal of Geophysical Research*, *110*, A09206. https://doi.org/10.1029/2004JA010708

Wygant, J. R., Cattell, C. A., Lysak, R., Song, Y., Dombeck, J., McFadden, J., et al. (2005b). Cluster observations of an intense normal component of the electric field at a thin reconnecting current sheet in the tail and its role in the shock-like acceleration of the ion fluid into the separatrix region. *Journal of Geophysical Research*, *110*, A09206. https://doi.org/10.1029/2004JA010708

Zong, Q.-G., Wilken, B., Woch, J., Mukai, T., Yamamoto, T., Reeves, G. D., et al. (1998). Energetic oxygen ion bursts in the distant magnetotail as a product of intense substorms: Three case studies. *Journal of Geophysical Research*, *103*(A9), 20,339–20,363. https://doi.org/10.1029/97JA01146